LA-UR -80-2039

CONF-800767--2

TITLE: APPLICATION OF MOOT TO SCATTERING OF ELASTIC WAVES FROM COMPOUND INCLUSIONS

MASTER

AUTHOR(S): William M. Visscher

SUBMITTED TO: DARPA/AFML Review of Progress in Quantitative NDE, La Jolla, California July 14 - 17, 1980

University of California

LOS ALAMOS SCIENTIFIC LABORATORY
Post Office Box 1663 Los Alamos, New Mexico 87545
An Affirmative Action/Equal Opportunity Employer

UNITED STATES
DEPARTMENT OF ENERGY
CONTRACT W-7405-ENG-36

APPLICATION OF MOOT TO SCATTERING OF ELASTIC WAVES FROM COMPOUND INCLUSIONS

William M. Visscher
Theoretical Division
Los Alamos Scientific Laboratory
University of California
Los Alamos, New Mexico 87545

ABSTRACT

We show how MOOT (method of optimal truncation, a convergent T-matrix scheme) can be used to calculate elastic wave scattering from compound inclusions; i.e. inclusions which themselves contain flaws - inclusions, voids, or cracks. The general equations are derived, and they are solved for a particular axially-symmetric case - a cracked spherical inclusion immersed in fluid. The crack edge is a circle on the equatorial plane; the crack can extend either inward to the center or outward to the surface of the sphere. Numerical results are given for scattering of acoustic waves from cracked spheres of various materials. Cracked spheres can be fabricated relatively easily, and may be useful in NDE calibrations.

INTRODUCTION

An experimental technique often used in ultrasonic measurements is to immerse an object in a tank of water and study it by scattering acoustic waves from it, the fluid effectively providing a coupling between the transducers and the object. In principle, one can determine all of the structural features of the object in this way. For NDE applications in particular, information is needed about internal flaws such as voids, inclusions, or cracks and about surface cracks and irregularities.

Because the crack is the most common and potentially the most dangerous defect in manufactured items, and the sphere is the simplest shape imaginable, a cracked sphere would seem to be a useful prototype of a compound inclusion. It is relatively easy to fabricate in practice and to compute scattering from, and could serve as a calibration standard, both experimentally and theoretically.

In this paper we will develop a general formalism with which the elastic wave equation can be solved for a system in which a compound inclusion is immersed in a host medium. The host medium may be either a fluid or an elastic solid, the compound inclusion may be complex and the generalization of the theory will be obvious, but we will calculate only included elastic spheres with cracks on their equatorial planes. The crack edges are circular, with the cracks extending either out to the surface or in to the center (see Fig. 1).

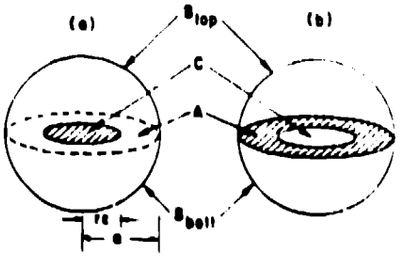

Fig. 1 Cracked spheres. The interior crack (a) has free boundaries; the peripheral crack (b) is fluid-filled. The equatorial plane is divided into a circle (C) and an annulus (A). The top and bottom hemispheres are called S_{top} and S_{bott}.

We will present a brief review of the computational method which we use. It is a straightforward extension of MOOT (method of optimal truncation) which was developed earlier.[1,2,3] We will show how to handle inclusions containing voids as well as internally and peripherally cracked inclusions.

Numerical results for scattering of acoustic waves from cracked spheres immersed in water are given in the final section. Both internal and surface cracks are considered. Results are shown for different crack sizes and are compared with scattering from uncracked spheres. The effects of material properties (acoustic impedances and propagation velocities) on the sensitivity of scattering to internal flaws are very important and probably will be the most stringent limitations on practical applications.

GENERAL DEVELOPMENT

The idea of MOOT will be explained for the simple case of a void within an inclusion, illustrated in Fig. 2. The vector displacement field

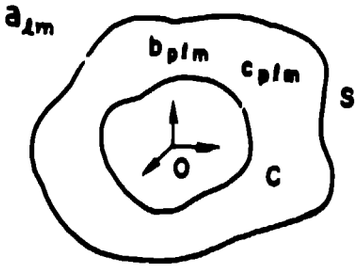

Fig. 2 A void (surface C) within an inclusion (surface S) immersed in a fluid. The displacement outside S consists of a plane wave plus outgoing partial waves (coefficients $a_{\ell m}$); inside S it is expanded in regular (coefficients $b_{p\ell m}$) and irregular (coefficients $c_{p\ell m}$) eigenfunctions of the elastic wave equation. The origin of coordinates is always taken inside C.

in the fluid outside the inclusion is expanded in outgoing eigenvectors of the acoustic wave equation,

$$\vec{S} = \sum d_{\ell m}\vec{S}_{\ell m} + \sum a_{\ell m}\vec{S}^{+}_{\ell m}, \tag{1}$$

where the $\vec{S}_{\ell m}$'s are given by

$$\begin{aligned}\vec{S}_{\ell m} &= k^{-1}\vec{\nabla} j_\ell Y_{\ell m}(\theta,\phi)\\ \vec{S}^{+}_{\ell m} &= k^{-1}\vec{\nabla} h^{+}_\ell Y_{\ell m}(\theta,\phi)\end{aligned} \tag{2}$$

with $k^2 = \rho\omega^2/\lambda$, $d_{\ell m} = 4\pi i^\ell Y^*_{\ell m}(\theta_0\phi_0)$. $\theta_0\phi_0$ are the spherical angles of the direction of the incident plane wave

$$\vec{S}_{inc}(\vec{r}) = k^{-1}\vec{\nabla} e^{i\vec{k}_0\cdot\vec{r}} = \vec{\nabla}\sum d_{\ell m} j_\ell(r) Y_{\ell m}(\theta,\phi), \tag{3}$$

λ is the fluid bulk modulus, $j_\ell(kr)$ is the regular spherical bessel function, and $h^{+}_\ell = j_\ell + iy_\ell$. The problem is to determine the as yet unknown coefficients $a_{\ell m}$, which we do as follows.

The displacement field inside the inclusion is

$$\vec{S}' = \sum b_{p\ell m}\vec{S}'_{p\ell m} + c_{p\ell m}\vec{S}'_{p\ell m}, \tag{4}$$

where $\vec{S}'_{p\ell m}$ for p = 1 (longitudinal polarization) is as given in (2) but with $k_L = \rho'\omega^2/(\lambda'+2\mu')$, and for p = 2,3 (transverse polarizations) is as given in ref. 2 but with $k_T = \rho'\omega^2/\mu'$, μ' being the shear modulus. $\vec{S}'_{p\ell m}$ is identical to $\vec{S}'_{p\ell m}$ except y_ℓ (spherical bessel function irregular at origin) is substituted for j_ℓ. The extra complexities of (4) are necessitated by the facts that the inclusion, being a general isotropic elastic material, can support shear stresses and therefore transversely polarized waves, and that no radiation condition (outgoing scattered waves at infinity) constrains the interior field, so that both regular and irregular bessel functions are needed.

The stress tensor σ_{ij} is formed by differentiating S_i in the usual way. When it is contracted with the unit normal n to a surface, the surface traction $t_i = \sum\sigma_{ij}n_j$ results:

$$\vec{t} = 2\mu(\hat{n}\cdot\vec{\nabla})\vec{S} + \mu\hat{n}\times(\vec{\nabla}\times\vec{S}) + \lambda\hat{n}\vec{\nabla}\cdot\vec{S} \tag{5}$$

A surface traction vector $\vec{t}_{p\ell m}$ corresponds to each $\vec{S}_{p\ell m}$. Because $\mu = 0$ in the fluid outside, only p = 1 exists there; all 3 polarizations usually contribute inside the inclusion.

The boundary conditions are expressed in terms of these vectors. On the surface of the void C, the surface traction vector vanishes

$$\vec{t}'(\vec{r}) = 0 \quad \vec{r} \text{ on } C, \tag{6}$$

and on the surface of the inclusion, the normal components of both displacement and surface traction are continuous

$$(\vec{S} - \vec{S}')\cdot\hat{n} = 0, \quad \vec{r} \text{ on } S \tag{7}$$

$$(\vec{t} - \vec{t}')\cdot\hat{n} = 0, \quad \vec{r} \text{ on } S \tag{8}$$

and the parallel components of surface traction on the inclusion vanish;

$$\vec{t}'\times\hat{n} = 0 \quad \vec{r} \text{ on } S. \tag{9}$$

Our task is to choose $a_{\ell m}$, $b_{p\ell m}$, and $c_{p\ell m}$ in such a way that (6), (7), (8), and (9) are satisfied simultaneously. This is obviously an impossible task (unless C and S happen to be concentric spheres, in which case we shall see that the problem is greatly simplified), so we will settle for second best, namely that (6), (7), (8), and (9) be satisfied in a least-squares sense. We form the following positive definite quadratic form

$$\begin{aligned}I = \alpha\int_C d\sigma|(6)|^2 + \beta\int_S d\sigma|(7)|^2 + \gamma\int_S d\sigma|(8)|^2\\ + \delta\int_S d\sigma|(9)|^2,\end{aligned} \tag{10}$$

where the integrals are over the surfaces C and S, α, β, γ, δ are positive constants, and the integrals are the absolute squares of the left hand sides of the referenced equations. Clearly I = 0 if and only if (6), (7), (8), and (9) hold.

One is always constrained by the realities of computation to truncate the sums in (1) and (4) to $\ell \le \ell_{max}$, where ℓ_{max} is usually quite small (~20 or less). Thus there are a finite number of coefficients $a_{\ell m}$, $b_{p\ell m}$, $c_{p\ell m}$, so that one always has I > 0. Our prescription for the choice of a, b, c is that I be minimized, viz.

$$\left.\begin{aligned}\frac{\partial I}{\partial a^*_{\ell m}} &= 0 \quad m = -\ell,-\ell+1\cdots\ell-1, \ell; \ \ell=0,\cdots\ell_{max}\\ \frac{\partial I}{\partial b^*_{p\ell m}} &= 0\\ \frac{\partial I}{\partial c^*_{p\ell m}} &= 0\end{aligned}\right\} p = 1,2,3;\ m = -\ell,\cdots\ell-1, \ell;\ \ell = 0,\cdots\ell_{max} \tag{11}$$

There are exactly as many equations in the set (11) as there are unknowns a, b, c, so in the absence of some unforeseen (and as yet unmaterialized) catastrophe (11) forms a set of linear equations which can be solved for the $a_{\ell m}$'s; they, in turn, give scattered amplitudes and cross-sections. Note that the equations (11) are <u>complex</u>, as are the a, b, c,'s; asterisk means complex conjugate. It is easy to see that as one increments ℓ_{max} to $\ell_{max}+1$, then $I(\ell_{max}+1) \le I(\ell_{max})$, so it follows that the approximation scheme results in a monotone convergent sequence with limit 0, if it is assumed that the partial wave series representation of the displacements and stresses converges.

We can write (10) out in vector notation;

$$I = a^{+}A_{aa}a + a^{+}A_{ab}b + c.c. + a^{+}A_{ac}c + c.c.$$
$$+ a^{+}A_{ad}d + c.c. + b^{+}A_{bb}b + b^{+}A_{bc}c + c.c.$$
$$+ b^{+}A_{bd}d + c.c. + c^{+}A_{cc}c + c^{+}A_{cd}d + c.c.$$
$$+ d^{+}A_{dd}d, \qquad (12)$$

where the A's are matrices whose elements are linear combinations of surface integrals; for example

$$(A_{aa})_{\ell m \ell' m'} = \int_S d\sigma [\beta \hat{n}\cdot\vec{t}^{*}_{\ell m}\hat{n}\cdot\vec{t}_{\ell' m'} + \gamma \hat{n}\cdot\vec{S}^{*}_{\ell m}\hat{n}\cdot\vec{S}_{\ell' m'}] \qquad (13)$$

as can be easily verified from (1), (7), (8) and (10). The linear equations (11) are obtained directly,

$$\frac{\partial I}{\partial a^{*}_{\ell m}} = \left(A_{aa}a + A_{ab}b + A_{ac}c + A_{ad}d\right)_{\ell m}, \qquad (14a)$$

$$\frac{\partial I}{\partial b^{*}_{p\ell m}} = \left(A_{ba}a + A_{bb}b + A_{bc}c + A_{bd}d\right)_{p\ell m} \qquad (14b)$$

$$\frac{\partial I}{\partial c^{*}_{p\ell m}} = \left(A_{ca}a + A_{cb}b + A_{cc}c + A_{cd}d\right)_{p\ell m}. \qquad (14c)$$

It might be pointed out that the A matrices in (14a,b,c) are mostly not square; A_{ba}, for example, has about 3 times as many rows as columns because 3 polarizations are usually allowed in the elastic inclusion versus only 1 in the fluid. This causes no problems in the matrix algebra one might do to solve for $a_{\ell m}$; row and column lengths always match properly in matrix multiplications, of course, and matrices which need to be inverted are always square.

The choice of the positive multipliers α, β, γ, δ in (10) is not critical, in fact it is irrelevant as $\ell_{max} \to \infty$. One can make a plausible argument[3] that a reasonable choice is unity for stress integral multipliers (α, β, δ) and minimum of ($\lambda^2 k^2, \lambda^2/a^2$) for displacement integral multipliers (γ).

Important simplifications occur in (14) if certain symmetries hold. First, if the scatterer S, C has an axis of symmetry it can be chosen to be the z-axis and all the A matrices are diagonal in m. Then (14) can be solved for each value of $m = 0, 1, \cdots \ell_{max}$ successively, which affords a great simplification and computing economy. If, in addition, the scatterer has complete rotational symmetry, i.e. S and C are concentric spheres, then the A matrices are in addition diagonal in ℓ. In this case (14) degenerates for each (ℓ,m) into a set of 5 simultaneous linear equations for one $a_{\ell m}$, two $b_{p\ell m}$'s, and two $c_{p\ell m}$'s (only p = 1 and p = 3 contribute for $\ell > 0$; if $\ell = 0$ only p = 1 does), so the problem becomes trivial to solve (with a computer) because one needs only to compute coefficients for and solve inhomogeneous linear systems of order 5.

More challenging is the problem we have set out to solve in this note, namely the cracked sphere illustrated in Fig. 1. Again the displacement is expanded outside the sphere as in (1), but now we need separate expansions in the top and bottom hemispheres

$$\vec{S}'_b = \sum b_{p\ell m}\vec{S}'_{p\ell m} \quad \text{(top)} \qquad (15b)$$

$$\vec{S}'_c = \sum c_{p\ell m}\vec{S}'_{p\ell m} \quad \text{(bottom)}, \qquad (15c)$$

where, in contrast to the case of the inclusion Eq. (4), only the regular basis functions are needed. The boundary conditions to be satisfied are that on the top and bottom hemispheres the normal displacements and surface tractions are continuous, and the parallel components of surface traction vanish. In the equatorial plane welded boundary conditions (continuous displacement and surface traction) are imposed on A in Fig. (1a) and on C in Fig. (1c), while free boundary conditions (vanishing surface traction) prevail on C in Fig. (1a) (open crack) and slippery boundary conditions (continuous normal components of displacement and surface traction, zero parallel components of surface traction) hold on A in Fig. (1b). So the interior crack is "clear" and the peripheral crack is "fluid-filled".

A positive definite linear combination of surface residuals like Eq. (10) can now be formed; it will have more terms because there are now more surface segments to consider, and the boundary conditions are different. But the bilinear form in a, b, c, and d is still Eq. (12), and the linear equations (14a,b,c) are unchanged. The matrix elements A will be different; like (13) they can be written down by inspection and evaluated numerically. Then Eqs. (14a,b,c) can be solved straightforwardly on a computer. One can significantly reduce the task of the computer by recognizing that the coefficients $c_{p\ell m}$ are simply related to $b_{p\ell m}$ because of the symmetries of the geometry.[3]

NUMERICAL RESULTS

Elastic properties and densities impose some drastic constraints on the materials which can be studied by ultrasonic immersion. This is illustrated on Fig. 3 which shows backscattering in water from various real and imagined spheres (without cracks). The dot-dash curve is backscattering from a tungsten carbide sphere. Tungsten carbide is so stiff (see Table I) that at these frequencies its scattering is identical, to the resolution of the graph, to that of a rigid sphere of the same density. One could not see the effects of flaws without going to much higher frequencies. A critical parameter here is the acoustic impedance mismatch with that of water, which can from Table I be seen to be extreme; the mismatch is a factor of 65. More hopeful is the case of aluminum, the solid curve of Fig. 3. With the elastic constants tripled one gets the dashed curve, which might marginally be distinguished experimentally from the solid one. The case of lucite, shown in the solid curve of Fig. 4, is much better, by comparison with the dashed curve, which is a fictitious material with the density of lucite and the elastic constants of tungsten carbide. The backscattering

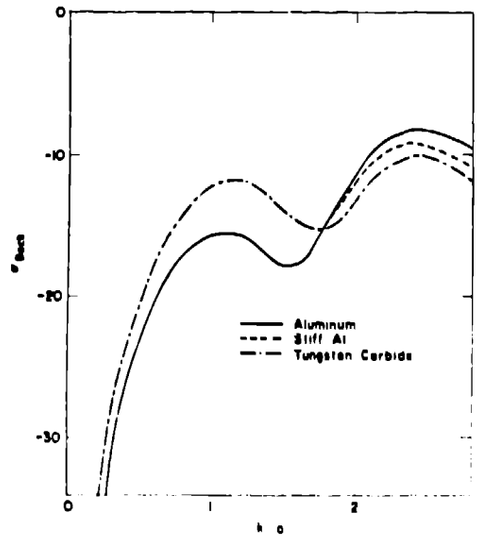

Fig. 3 Backscattering of acoustic waves from spheres in water. To the resolution of the graph, completely rigid tungsten carbide would be the same as the dot-dash curve, and completely rigid aluminum would be the same as the dashed curve.

Material	$\lambda\times10^{-10}$	$\mu\times10^{-10}$	$\rho\times10^{-3}$	v_{long}	ρv_{long} $\times10^{-7}$
Water	.197	0	1.0	1404	.140
Polyethylene	.288	.026	.90	1950	.176
Lucite	.562	.143	1.18	2680	.317
Magnesium	2.56	1.62	1.74	5770	1.00
Pyrex	2.3	2.5	2.32	5640	1.31
Aluminum	6.1	2.5	2.70	6420	1.73
Beryllium	1.6	14.7	1.87	12890	2.41
Titanium	7.8	4.4	4.50	6070	2.73
Tungsten Carbide	17.1	22.0	13.8	6655	9.18

Table I Elastic properties of various materials in MKS units. The final column is the acoustic impedance.

changes by more than a factor of 100 at the ka = 1.6 peak. Effects of this order should be easily measurable.

We have calculated scattering from various cracked lucite spheres. Some of the results are shown in Figs. 5, 6, and 7. Figure 5 pictures the backscattering cross-section $\sigma_{back}(\theta_0=0)$ for incident angle $\theta_0 = 0$ for a lucite sphere with an interior "clear" crack of radius .5a (solid line), and the dashed and dot-dash lines are $\sigma_{back}(\theta_0 = 45)$ and $\sigma_{back}(\theta_0 = 90)$ respectively. This crack covers 25% of the area of the equatorial plane; its effects on $\sigma_{back}(\theta_0 = 90)$ are fairly small, as can be seen by comparing with Fig. 4. The deviation of the solid, dot-dash, and dashed lines from each other can be considered the flaw signature; in the absence of the crack they will, of course, condense to one curve, the solid line of Fig. 4.

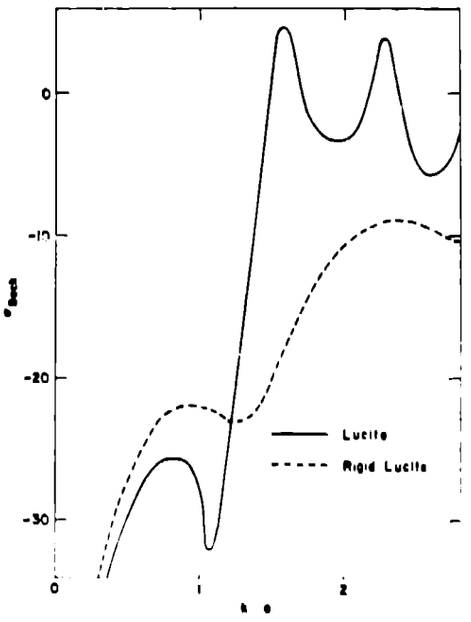

Fig. 4 Backscattering of acoustic waves from lucite sphere in water, and from a fictitious sphere with the density of lucite but with the elastic constants of tungsten carbide.

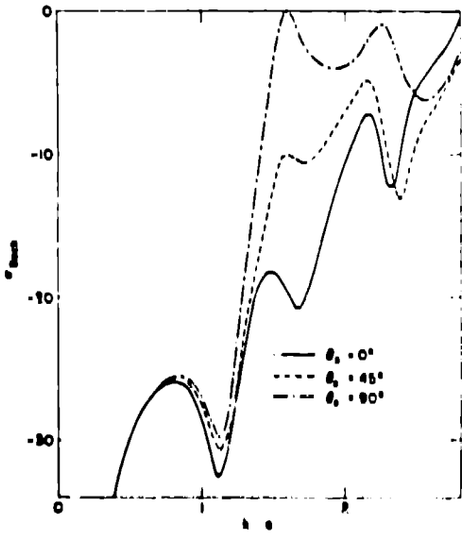

Fig. 5 Backscattering of acoustic waves from a cracked lucite sphere in water. The crack is "clear", circular with half the radius of the sphere. The incident angle θ_0 is the polar angle relative to the axis of symmetry.

Increasing the radius of the crack to .8a so that it covers half the equatorial plane results in the backscattering shown in Fig. 6. Quite similar to the curves of Fig. 5, these cross-sections can be distinguished by the much deeper interference

minima at $k_L a = 2.3$.

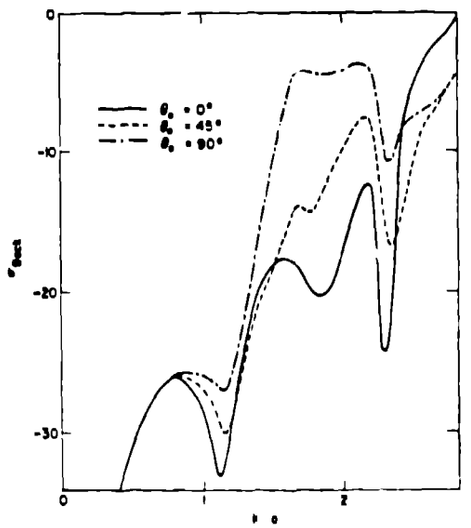

Fig. 6 Like Fig. 5, but the radius of the sphere is .7a, so it covers half the area of the equatorial plane.

The result of circumcising the sphere equatorially to a depth of .3a (so the resulting fluid-filled crack has area half that of the equatorial plane). The dot-dash curve here ($\sigma_{back}(\theta_0 = 90)$) is nearly identical to the unflawed sphere, and the quantitative changes for $\theta_0 = 0$ and $\theta_0 = 45$ are generally less than for the interior crack. This surface crack is much harder to detect than the interior clear crack of the same area (cf. Fig. 6).

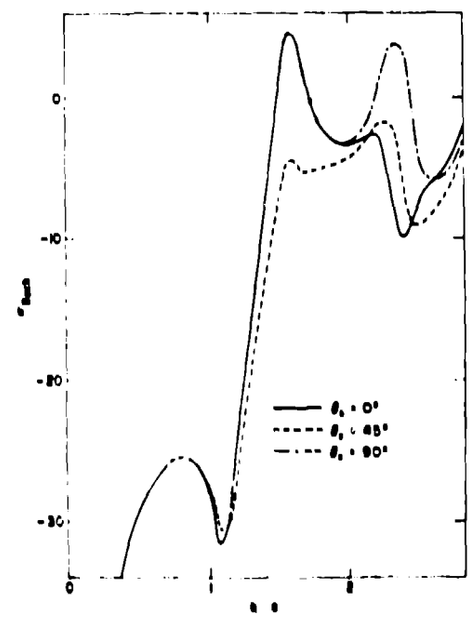

Fig. 7 Backscattering from a lucite sphere with a fluid-filled surface crack of depth .3a around its equator.

REFERENCES

1. William M. Visscher, J. Appl. Phys. 51, 825 (1980).
2. William M. Visscher, J. Appl. Phys. 51, 835 (1980).
3. William M. Visscher, to be published in Wave Motion.

Support for this research has been provided by the United States Department of Energy.